Eur. Phys. J. D **45**, 279–287 (2007)
DOI: 10.1140/epjd/e2007-00265-7

THE EUROPEAN PHYSICAL JOURNAL D

Dissociation channels of silver bromide cluster Ag_2Br, silver cluster Ag_3 and their ions studied by using alkali metal target

H. Nagao[1], K. Awazu[1], S. Hayakawa[2,a], K. Iwamoto[2], M. Toyoda[3], and T. Ichihara[3]

[1] Division of Sustainable Energy and Environmental Engineering, Graduate School of Engineering, Osaka University, 2-1 Yamadaoka, Suita, 565-0871 Osaka, Japan
[2] Department of Chemistry, Graduate School of Science, Osaka Prefecture University, 1-1 Gakuencho, Nakaku, Sakai, 599-8531 Osaka, Japan
[3] Department of Physics, Graduate School of Science, Osaka University, 1-1 Machikaneyama, Toyonaka, 560-0043 Osaka, Japan

Received 28 June 2007 / Received in final form 14 August 2007
Published online 19 September 2007 –

Abstract. Various dissociation channels of silver bromide cluster ion Ag_2Br^+ and silver cluster ion Ag_3^+ were observed in high-energy collisionally-activated dissociation (CAD) using a Cs target. The fragment patterns of the high-energy CAD were compared with those of the metastable dissociation and low-energy CAD. The difference in the fragment patterns between the high-energy CAD and the other dissociation methods was explained in terms of the internal energy distributions. The dissociation mechanisms of neutral silver bromide cluster Ag_2Br and silver cluster Ag_3 were also investigated by charge inversion mass spectrometry using the Cs target. While the fragment ions $AgBr^-$ and Ag_2^- were dominantly observed in the charge inversion spectrum of Ag_2Br^+, the undissociated ion Ag_3^- was observed as a predominant peak in the case of Ag_3^+. The dissociation behavior of Ag_2Br^* can be explained on the basis of the calculated thermochemical data. Contrary to this, the predominant existence of the undissociated Ag_3^- cannot be explained by the reported thermochemical data. The existence of undissociated Ag_3^- suggests that the dissociation barrier is higher than the internal energy of Ag_3^* (theoretical: 1.03 eV, experimental: 2.31 eV) estimated from the ionization potentials of Ag_3 and Cs.

PACS. 36.40.Wa Charged clusters – 34.70.+e Charge transfer – 36.40.-c Atomic and molecular clusters

1 Introduction

Silver bromide has been studied for many years in the condensed phase due to its important implications in the photographic process. In order to clarify the reactions involved in the process, both of silver and silver bromide clusters have been widely investigated [1]. The silver clusters have also received particular attention because of a theoretical interest in the fact that a silver atom has electrons in the outer 4*d*-orbitals energetically overlapped by the partially filled 5*s*-orbital.

Silver trimers have been a main topic of a large number of earlier experimental [2–8] and theoretical [1,9–18] studies. Among other experimental works on small silver clusters, Spasov et al. reported the fragmentation patterns, cross sections, and dissociation energies of anionic silver clusters Ag_n^- by using the energy-resolved collisionally-activated dissociation (CAD) method [6]. The main reaction channels were found to be the eliminations of a Ag atom and a dimer Ag_2, with the dimer less favored for odd n values. Dissociation energies for the loss of a silver atom showed a strong odd-even-dependent alternation against n. Handschuh et al. studied photoelectron spectra of silver anion clusters by exciting at different photon energies in order to explore the electronic structures of various silver clusters [5]. The shaper spectral patterns of the silver clusters observed in their experiments as compared with those of the corresponding alkali metal clusters might be due to the stronger bonding in the silver clusters. This can be interpreted as the result of overlapping of the outer 4*d* and 5*s* orbitals, which gives rise to van der Waals type attractive force. Recently the symmetric and antisymmetric vibrational bands of neutral Ag_3 were assigned by using far-infrared spectroscopy by Fielicke et al. [8]. The energy levels of the silver clusters and their ions were theoretically evaluated [1,9–18].

Regarding the dissociation methods, electronic mechanism (electronic excitation) and impulsive mechanism (momentum transfer) about initial steps of collision induced dissociations have been discussed using position sensitive detections [19–24]. Barat and coworkers differentiated between electronic and impulsive mechanism in the collisional activated dissociation for the collisions of cluster ions with H_2 or rare gas targets by detecting both fragment ions and fragment neutrals [20–24]. After the excitation by impulsive mechanism, the excited molecules

[a] e-mail: hayakawa@c.s.osakafu-u.ac.jp

dissociate through the internal collisions in the second step. For the experiment using metal targets, de Bruijn et al. [19] indicated that dissociative electron transfer initiated by the electron mechanism dominated molecular dissociation. One of the authors also confirmed the electron transfer mechanism by charge inversion mass spectrometry using alkali metal targets [25]. Femtosecond negative to neutral to positive (NeNePo) spectroscopy was used to study the structural dynamics of the neutral cluster Ag_3 [26–28]. The wave packet dynamics along the coordinate of the linear-to-triangular rearrangement on the ground state potential surface was investigated in detail by Boo et al. [27]. These authors commented on the splitting of the degeneracy of the neutral Ag_3 states due to a strong Jahn-Teller effect. Leisner et al. [28] indicated an apparent loss of vibrational coherence by the ultrafast intramolecular vibrational energy redistribution interpretable as an intermolecular collision process. These experimental results have been confirmed by the theoretical studies [29–33].

Mixed clusters have been also an object of recent researches. Metastable fragmentation channels for anionic and cationic silver bromide clusters were examined by L'Hermite et al. [34,35] and were compared with ab initio DFT results [36,37]. They indicated that the fast fragmentation induced by a UV laser made the cations lose a bromine atom more easily than a silver ion and that the negative ions mass spectra contained species with more silver atoms than required by stoichiometry. Contrary to the silver clusters, dissociation processes of the neutral silver bromide clusters are not known to our best knowledge.

In this paper, we investigated the dissociation processes of the cations of both silver trimer (Ag_3) and silver bromide cluster (Ag_2Br) by high-energy CAD spectra measured by using the Cs metal target. As has been confirmed from their internal energy distributions [38,39], the dissociation processes in the high-energy CAD spectra do not depend on which of alkali metal and rare gas targets is employed [39,40]. The dissociation processes of their neutrals were investigated by charge inversion mass spectrometry with alkali metal targets, which has been developed in our laboratory [39,41,42]. Charge inversion mass spectrometry can provide us with direct information about the dissociation pathway of energy-selected neutral clusters formed by the near-resonant neutralization of the corresponding cation clusters [39,41,42]. The reaction process involved in this spectroscopy corresponds to a reverse process of NeNePo [26–28]. Dissociation mechanisms of small clusters are particularly interesting from the viewpoint of chemical reactivity, because the small clusters often exhibit significantly different physical and chemical properties from those in the isolated molecular state or in the condensed phase. In the present work, the dissociation mechanisms of the excited silver trimer Ag_3 and silver bromide cluster Ag_2Br were investigated by the charge inversion mass spectrometry. The obtained charge inversion mass spectra showed a significant difference between Ag_3 and Ag_2Br. The difference is discussed in terms of the energy levels of the respective excited neutral clusters and relevant fragments.

2 Experimental section

Mass-selected positive ions were made to collide with an alkali metal target, and the resulting negative ions formed upon two successive single-electron transfers were mass analyzed by using an MS/MS instrument. The experimental setup was described in detail elsewhere [43]. Briefly, silver bromide cluster ions and silver cluster ions were generated by fast atom bombardment (FAB) on a pressed pellet of silver bromide purchased from Wako. The pellet was sputtered by Xe atoms bombardment typically at 8 keV. The Xe atoms were obtained by resonant electron transfer of Xe^+ ions which were produced by a discharge type ion source with a discharge current of 20 mA. The ions generated by FAB were accelerated to the translational energy of 5 keV. Precursor ions were mass-selected by a JEOL JMS-HX110 double-focusing mass spectrometer (MS-I). The mass-selected precursor ions were led into a 3.7 cm long collision cell located at the exit of MS-I. The alkali metal was introduced into the collision cell as a vapor from a reservoir through a ball valve. In this work, cesium (Cs) was used as a target vapor. The temperatures of the collision cell, the ball valve, and the reservoir were controlled to adjust the density of the Cs vapor in the collision cell. Neutralization, dissociation, and negative ion formation took place in the collision cell containing the Cs vapor. The negative ions were mass analyzed by a spherical electrostatic analyzer (ESA) with a central radius of 216 mm (MS-II). The mass-analyzed ions were detected by a 9 kV post-acceleration secondary electron multiplier, which could detect both positive and negative ions upon the application of an appropriate polarity. Charge inversion spectra were measured by mass-analyzing the negative ions exiting from the collision cell by scanning the ESA voltage. By changing the polarities of MS-II and multiplier, the CAD spectra of the positive ions exiting from the collision cell were measured in the same way as for the negative ions.

3 Results and discussion

3.1 Silver bromide cluster Ag_2Br

A CAD spectrum and a charge inversion spectrum of the silver bromide cluster ion $^{107}Ag_2{}^{79}Br^+$ (m/z 293) measured with the Cs target are shown in Figures 1a and 1b, respectively. Mono-isotopic precursor ions were selected. A clear difference is recognized between the CAD spectrum and the charge inversion spectrum of Ag_2Br^+. In the CAD spectrum (Fig. 1a), the peak for the undissociated ion Ag_2Br^+at m/z 293 is by far the strongest and well exceeds the upper limit of the scale on the vertical axis. The high intensity of this Ag_2Br^+ peak is attributed to the precursor ion that did not interact with the target. The peaks located at m/z 107, 186, and 214 are observed dominantly and are associated with Ag^+, $AgBr^+$, and Ag_2^+ ions resulting from the loss of AgBr, Ag, and Br from the precursor ion Ag_2Br^+, respectively. The peak located at m/z 79 and associated with Br^+ ion is scarcely observed.

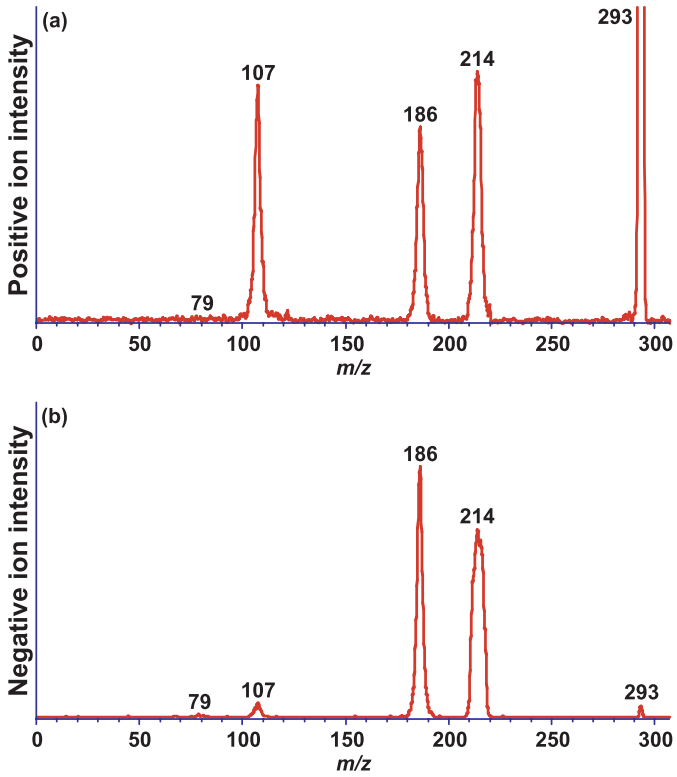

Fig. 1. CAD spectrum (a) and charge inversion spectrum (b) of Ag_2Br^+ (m/z 293). The ion was formed by fast atom bombardment (FAB). The target element was Cs and the collision energy was 5 keV.

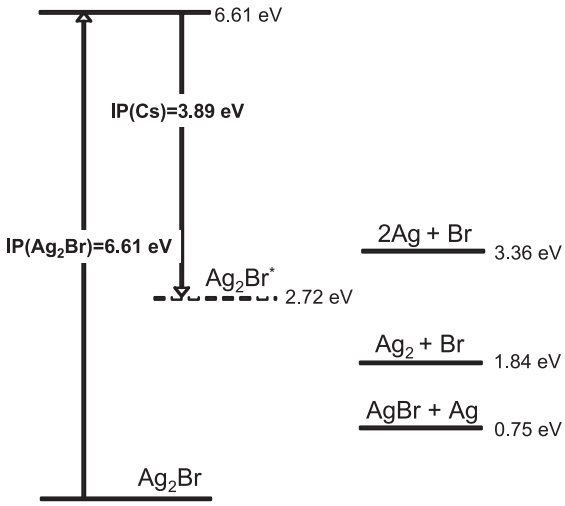

Fig. 2. Heats of formation of the neutral and cationic forms of Ag_2Br, relative to that of Ag_2Br in the ground state. The thermochemical data are taken from references [36,37]. The dashed line shows the energy level predicted by the near-resonant neutralization with a Cs target.

The investigation by L'Hermite et al. [34] showed that only the peak associated with Ag^+ formed by the loss of AgBr was observed in the metastable fragmentation of Ag_2Br^+. The lowest dissociation channel of Ag_2Br^+ derived from ab initio DFT calculations is in a satisfactory agreement with their experimental results, and is able to account for the dissociation channel of Ag_2Br^+ which dissociates preferentially into $Ag^+ + AgBr$. In contrast to the metastable fragmentation, the peaks associated with Ag^+, $AgBr^+$, and Ag_2^+ were dominantly observed in the present high-energy CAD spectrum of Ag_2Br^+. The difference in the dissociation channels between the high-energy CAD and the metastable fragmentation was explained by the internal energy distribution in Ag_2Br^{+*}. The energy distribution of the metastable ions produced thus is very narrow and centers closely around the lowest dissociation energy limit. The low internal energy available in the metastable fragmentation yields only the peak associated with Ag^+ formed from the loss of AgBr. On the contrary to this, high-energy CAD has a maximum of distribution at the low energy limit and shows a long tail extending to the higher energy beyond several electron volts [38,45–48]. The broad and higher internal potential energy of Ag_2Br^{+*} examined in the present work allows many dissociation channels such as the loss of any one of Br, Ag, AgBr, and Ag_2.

The charge inversion spectrum of the silver cluster ion Ag_2Br^+ (m/z 214) with the Cs target is shown in (Fig. 1b). The peaks located at m/z 186 and 214 are associated with $AgBr^-$ and Ag_2^-, respectively and are the dominant peaks in the charge inversion spectrum (Fig. 1b), whereas the peak at m/z 293 associated with the undissociated ion Ag_2Br^- is hardly observed. The peaks associated with Br^- and Ag^- are also observed at m/z 79 and 107, but their intensities are much weaker than those for Ag_2^- and $AgBr^-$. In order to elucidate the mechanism of dissociation of the excited cluster Ag_2Br^*, we compared our experimental results with the thermochemical data available. These thermochemical data for the Ag_2Br system are illustrated in Figure 2 together with the energy levels associated with the near-resonant neutralization using the Cs target. The heats of formation of Ag_2Br^+, Ag_2Br, and those of the fragments formed via dissociation of Ag_2Br, relative to that of the ground state of the Ag_2Br neutral are given in Figure 2. Since the ionization potential and dissociation energies of Ag_2Br have not been reported experimentally, theoretically calculated values are used. Most of the data are taken from references [36,37]. The bond dissociation energies of the Ag-Br and Ag-Ag bonds are also taken from reference [37]. In our previous studies using thermometer molecules, such as $W(CO)_6$, which lose CO ligands consecutively when they have enough energy to dissociate [38,39,49], it was demonstrated that the neutralization step in the charge inversion process is via near-resonant electron transfer. Therefore, when this is the case, the energy level of the neutral species formed should be lower than the level of the corresponding precursor ion by an amount equal to the ionization energy of the target atom. The energy level associated with the resonance process with the Cs target is shown as a dashed line (at 2.72 eV) in Figure 2. Dissociations into $Ag_2 + Br$ and $AgBr + Ag$ are energetically allowed when the neutralization is a near-resonant process, because the energy level of $Ag_2 + Br$ (at 1.84 eV)

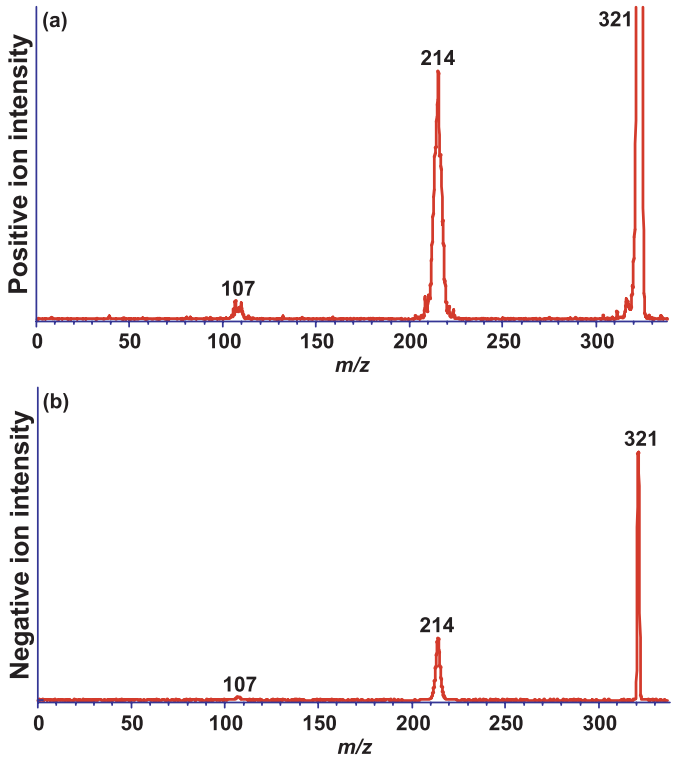

Fig. 3. CAD spectrum (a) and charge inversion spectrum (b) of Ag_3^+ (m/z 321). The ion was formed by fast atom bombardment (FAB). The target element was Cs and the collision energy was 5 keV.

and AgBr + Ag (at 0.75 eV) are lower than that of Ag_2Br^* (at 2.72 eV) by 0.88 and 1.97 eV, respectively, as is shown in Figure 2. The dissociation into 2Ag + Br (at 3.36 eV) is, however, energetically impossible, since it is 0.64 eV higher than that of Ag_2Br^* as is also shown in Figure 2. From a comparison with the thermochemical data, all the fragment ions observed in the charge inversion spectrum are supposed to be formed by the dissociation of Ag_2Br^* into AgBr + Ag and Ag_2 + Br. The very weak intensity observed for the undissociated Ag_2Br^- ion indicates that the excited neutral species Ag_2Br^* has sufficient internal energy to dissociate before the second electron transfer occurs. Thus, the dissociation behavior of Ag_2Br^* revealed in the charge inversion spectrum is explained by the calculated thermochemical data.

3.2 Silver cluster Ag_3

The CAD and charge inversion spectra of the silver cluster ion $^{107}Ag_3^+$ (m/z 321) recorded with the Cs target are shown in Figure 3. The fragment peaks associated with Ag^+ (m/z 107) and Ag_2^+ (m/z 214) are observed in the CAD spectrum (Fig. 3a), and the intensity of Ag^+ is much weaker than that of Ag_2^+. The strongest peak at m/z 321 was attributed to the undissociated precursor ion that did not interact with the target, as was done in analyzing the CAD spectrum of Ag_2Br^+ shown in Figure 2. The low-energy dissociation channel of the silver cluster ion Ag_3^+ determined by CAD using a Penning trap was reported by Kruckeberg et al. [7]. In their CAD experiment, the cyclotron motion of the cluster ions was excited by a 1 ms resonant excitation pulse and an argon gas pulse was directed into the trap volume. A storage period of 100 ms there allowed the clusters to collide with argon atoms and to decay to smaller neutral or ion fragments. In their low-energy and multiple-collision CAD experiment, the Ag_3^+ ions decayed predominantly into Ag^+ ions, which were presumably produced by the evaporation of silver dimer Ag_2. On the other hand, the dissociation energy of Ag_3^+ into $Ag_2^+ + Ag$ calculated theoretically by Huda et al. [17], is 2.374 eV and lower than that of 2.533 eV required for the dissociation into $Ag_2 + Ag^+$. In the high-energy CAD spectrum of Ag_3^+ measured in the present work, we observed the ion Ag_2^+, which was formed by loss of a Ag atom, as a predominant fragment peak. The differences in the dissociation channels between the low-energy and high-energy CAD can be again understood by considering the internal energy distribution in Ag_3^{+*}. High-energy CAD has a maximum of distribution at the low energy limit and shows a long tail extending to the higher energy beyond several electron volts [38,45–48]. For low-energy CAD, the energy distribution is controlled by changing the collision energy and the times of collisions, and both low-energy and high-energy tails are short [47]. Therefore, if the theoretical calculation of the dissociation energy of Ag_3^+ is relied on, then the higher preference of the lower-dissociation-energy channel of Ag elimination in the high-energy CAD experiment is explained by the internal energy distribution localized mostly in the low energy region.

The charge inversion spectrum of the silver cluster ion $^{107}Ag_3^+$ (m/z 321) measured with the Cs target is shown in Figure 3b. Peaks associated with Ag^-, Ag_2^-, and Ag_3^- are observed. The peak for the undissociated ion Ag_3^- is predominantly observed at m/z 321, whereas the peak at m/z 293 associated with the undissociated ion Ag_2Br^- was hardly observed in the charge inversion spectrum of Ag_2Br^+ ions (Fig. 1b). The predominant peak of undissociated Ag_3^-, which makes a great contrast to the case described above for Ag_2Br, is unusual, since the electronically excited species formed from their corresponding positive ions are not usually observed in charge inversion spectra because of their rapid fragmentations driven by sufficient internal energies. In the previous studies using the charge inversion mass spectrometry, undissociated charge inverted ions were observed only for atomic [50], C_2 and C_2H anions [51,52] formed by double-electron transfer in a single collision. When an alkali metal is used as a target, the double-electron transfer in a single collision is much less probable than successive single-electron transfers in two collisions, as was discussed previously by one of the present authors [42,50]. The successive electron transfers do not often yield stable anions, even if the intermediate neutral clusters or molecules have positive electron affinities, as has been known in the case of vinylidene [53,54] or CH_n [55]. Only one exception for the formation of negative ions by the successive single-electron

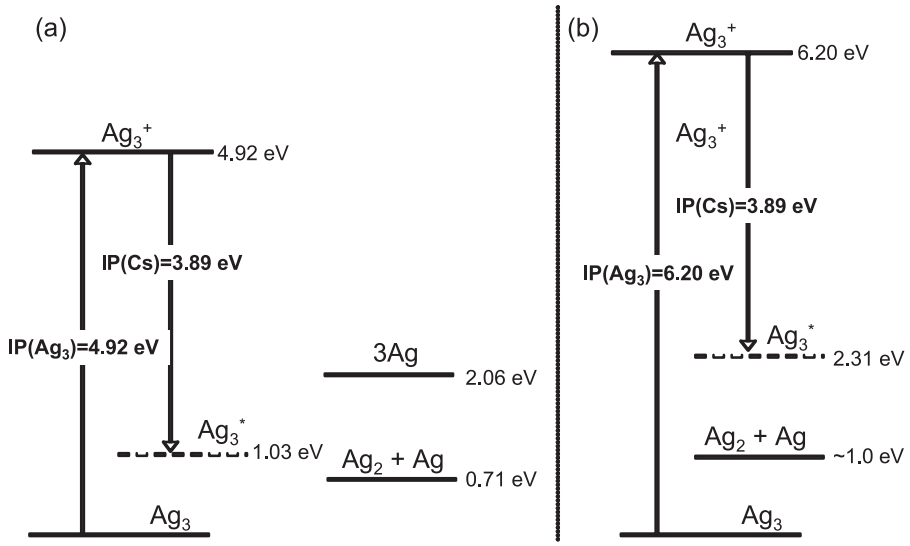

Fig. 4. Heats of formation of the neutral and cationic forms of Ag_3, and their fragments relative to that of Ag_3 in the ground state. Panels (a) and (b) show the theoretical and experimental values, respectively. The thermochemical data are taken from references [3,4,17]. The dashed lines show the energy levels predicted by the near-resonant neutralization with a Cs target.

transfers was observation of an undissociated anion of H-atom adduct Gly-Pro, in which the ring opening of the proline residue took place by N-Cα bond cleavage [56]. The small peaks at m/z 107 and 214 shown in (Fig. 3b) are associated with Ag and Ag_2, respectively, which are the fragments expected from the dissociation of Ag_3 into $Ag_2 + Ag$. The intensity difference between Ag^- and Ag_2^- results from a difference in the cross section for the negative ion formation as well as in the detection efficiency of a post-acceleration secondary multiplier. Such difference in the peak intensity between the complementary fragments has been observed for isomeric dichlorobenzenes [42,57,58] and isomeric chlorophenols [59].

In order to clarify the mechanism of the process from the positive ion Ag_3^+ to the negative ion Ag_3^- via successive single-electron transfers in two collisions, we compared the experimental results with the thermochemical data. The thermochemical data for the Ag_3 system were calculated by many researchers [1,9–18]. Recently calculated values reported by Huda et al. [17] are illustrated in Figure 4a. The energy level associated with the near-resonance neutralization with the Cs target is shown by a dashed line (at 1.03 eV) and is higher by 0.32 eV than that of Ag_2+Ag (at 0.71 eV) but 1.03 eV lower than that of 3Ag (at 2.06 eV). The thermochemical data show that the dissociation of Ag_3 into three Ag atoms is energetically impossible but the dissociation of Ag_3 into $Ag_2 + Ag$ is allowed. However, the predominant peak observed for Ag_3 in the charge inversion spectrum shown in Figure 3a indicates that the Ag_2-Ag bond cleavage in Ag_3^* is unfavorable. The thermochemical data based on the experimental work are also reported by Ho et al. [3] and Jackschath et al. [4] and these experimental values are given in Figure 4b. The vertical ionization energy of Ag_3 was obtained as 6.2 eV from an appearance energy by electron impact ionization [4], and the bond dissociation energy of Ag_2-Ag was estimated as 0.97 ± 0.16 eV using photoelectron spectroscopy of Ag_3^- [3]. Except these works, there are no experimental data available for both the ionization energy and bond dissociation energy of Ag_3. The differences in ionization energy and in the bond dissociation energy between the experimental and theoretical values are 1.3 eV and 0.3 eV, respectively, as is seen from Figure 4. Although a part of this large difference in the ionization energy between the experimental and theoretical values may be rationalized by ascribing it to the difference between the vertical and adiabatic values, the difference of 1.3 eV is still too large. The ionization energy evaluated from the appearance energy by electron impact [4] is not so reliable. For example, the observation of Ag_3^+ by two photon ionization at 410 nm in the NeNePo experiments reported by Boo et al. [27] indicates that the ionization energy is lower than 6.05 eV which is 0.15 eV smaller than the ionization energy determined by the electron impact method. The energy level of 2.31 eV by the near-resonant neutralization shown as the dashed line in Figure 5b is higher approximately by 1.30 eV than the experimental value for the dissociation into $Ag_2 + Ag$ (at ca. 1.0 eV). The thermochemical values evaluated from both theoretical and experimental values cannot explain the dominating presence of the undissociated ion Ag_3^- in the charge inversion spectrum.

3.3 Dissociation energies and mechanisms for the formation of undissociated Ag_3^-

By using the thermometer molecules, it has been demonstrated that the formation process of the negative ions in the charge inversion mass spectrometry proceeds via near-resonant neutralization with an alkali metal target, followed by spontaneous dissociation of the neutrals and the endothermic negative ion formation upon a second collision with the alkali metal target, as shown in the following reaction scheme (1) [38,39,42,49]

$$\begin{aligned} AB^+ + T &\rightarrow AB^* + T^+, \\ AB^* &\rightarrow A + B, \\ A\ (\text{or } B) + T &\rightarrow A^-\ (\text{or } B^-) + T^+, \end{aligned} \tag{1}$$

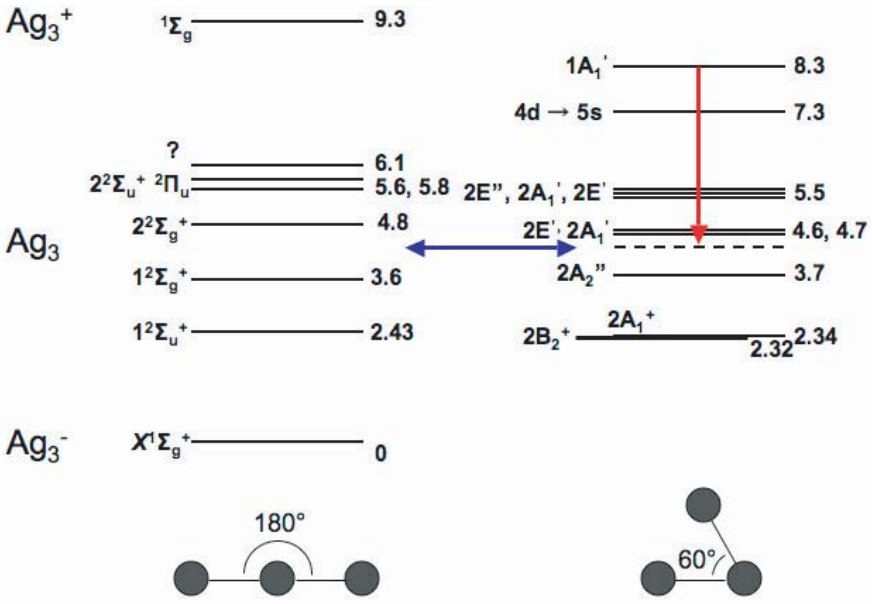

Fig. 5. Calculated transition energies of Ag_3^-, Ag_3, and Ag_3^+ along the bending coordinate. The thermochemical data are taken from reference [27].

where AB and T indicate a projectile and a target, respectively. The charge reversal reactions in the femtosecond negative to neutral to positive (NeNePo) spectroscopy in which an electron is photo-detached from a negative ion, followed by two-photon ionization to a positive ion [26–28], as shown in the following reaction scheme (2), correspond to the reverse processes to our charge inversion processes

$$\begin{aligned} AB^-(\text{linear}) + h\nu &\rightarrow AB(\text{linear}) + e^-, \\ AB(\text{linear}) &\rightarrow AB(\text{bent}), \\ AB(\text{bent}) + 2h\nu &\rightarrow AB^+ + e^-. \end{aligned} \quad (2)$$

A large number of theoretical calculations [1,9–18] have been performed to determine the structures and energies of silver trimers (Ag_3^-, Ag_3, and Ag_3^+) and it has been confirmed that Ag_3 and Ag_3^+ assume triangular forms at their global potential minima but Ag_3^- takes a linear form. The investigation using the femtosecond NeNePo spectroscopy suggested that the linear cluster Ag_3 produced by the photodetachment of the linear ion Ag_3^- rearranged into a triangular form on a 1 ps timescale due to a very low isomerization barrier as compared with that for the decomposition [26–28]. This very fast rearrangement was confirmed by a few theoretical works [29–33]. In the NeNePo experiment, Ag_3^+ ions were produced by the two-photon ionization of Ag_3 neutral clusters. The constant signal intensity of Ag_3^+ after 2 ps from the ionization preceded by the electron detachment of Ag_3^- indicated that an equilibrium between the linear and triangular forms of Ag_3 was achieved within a few ps [27,28].

The excited states of the linear and triangular forms of Ag_3 were also reported [1,10,14,15]. Figure 5 shows the calculated electronic energy levels of Ag_3^-, Ag_3, and Ag_3^+ along the bending coordinate taken from reference [27]. Typical collision interaction times for the neutralization in which the precursor ions are accelerated by 5.0 kV is in the range of 10^{-14} s. Since this time is significantly shorter than the time required for a conventional vibration ($\approx 10^{-13}$ s), the neutralization is expected to be a Franck-Condon process. Consequently, the geometry of the electronically excited cluster Ag_3^* is presumed to remain the same as that of the precursor ion Ag_3^+. As shown in Figure 5, the energy levels of $2E'$ (at 4.6 eV) and $2A_1'$ states (at 4.7 eV) of the triangular cluster Ag_3^* match the excitation energy (at 4.4 eV) required for the near-resonant neutralization with the Cs target, which is lower than the energy level of the precursor ion (at 8.3 eV) by an amount equal to the ionization energy of the Cs target (3.89 eV). Since the energy level is much higher than the isomerization barrier between the linear and triangular forms, the intramolecular rearrangement by ultra fast vibrational energy redistribution can occur on a ps time scale as reported in the NeNePo experiments [26–28]. As the average free time between the neutralization and anionization in the collision cell is 0.35 μs, the equilibrium between the linear and triangular forms is expected to be fully achieved provided that the dissociation does not take place because of the high dissociation barrier. On the basis of above discussion, we assumes that the linear cluster Ag_3 which has the higher electron affinity than that of the bent cluster captures another electron from the Cs target and, hence, the linear cluster ion Ag_3^- is observed in the charge inversion spectrum of Ag_3^+. From a comparison with the NeNePo experiments of Ag_3^-, it is presumed that Ag_3^* formed from Ag_3^+ by the near-resonant neutralization with the Cs target does not dissociate due to the energy barrier too high for the dissociation into $Ag_2 + Ag$ and, instead, Ag_3 does intramolecular rearrangement to the linear neutral cluster Ag_3, followed by negative ion formation on another collision with the target, as is expressed in the following

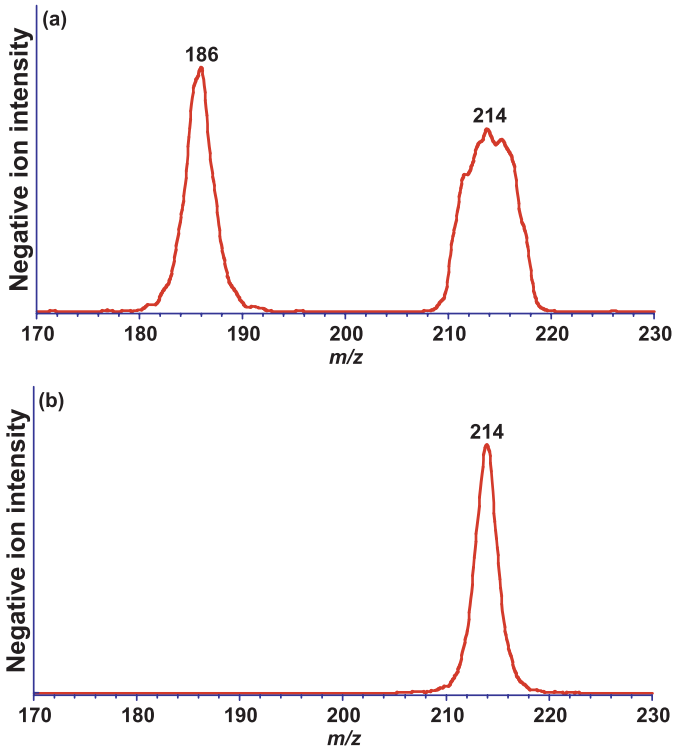

Fig. 6. Charge inversion spectra of the Ag_2Br^+ (m/z 293, Fig. 1) (a) and Ag_3^+ (m/z 321, Fig. 3) (b) enlarged in the range m/z 170–230.

reaction scheme (3)

$$\begin{aligned} AB^+(\text{bent}) + T &\rightarrow AB^*(\text{bent}) + T^+, \\ AB^*(\text{bent}) &\rightarrow AB^*(\text{linear}), \\ AB^*(\text{linear}) + T &\rightarrow AB^-(\text{linear}) + T^+. \end{aligned} \quad (3)$$

From the existence of the predominant peak for the undissociated cluster ion Ag_3^- in the charge inversion spectrum, we inferred that the energy barrier for the dissociation into $Ag_2 + Ag$ is higher than the energy level of Ag_3^* formed via near-neutralization with the Cs target, though the energy barrier theoretically calculated has not been reported so far.

3.4 Dissociation mechanism and structure of Ag_2Br^+

To see the peak shape more clearly, the charge inversion spectra of $^{107}Ag_2{}^{79}Br^+$ and $^{107}Ag_3^+$ expanded in the m/z 170–230 range are shown in Figures 6a and 6b, respectively. While in the case of Ag_3^+, the peak associated with Ag_2^- at m/z 214 in Figure 6b is sharp and its peak shape resembles a triangle, the peak at m/z 214 derived from Ag_2Br^+ shown in Figure 6a is broad and its band shape resembles a trapezoid. The width and profile of the fragment peaks of Ag_2^- show a clear dependence on precursor ion. In addition to this difference, the peak associated with $AgBr^-$ ions at m/z 186 is also sharp and has a triangular profile, as shown in Figure 6a. Such triangular profile is typical of the fragment peaks observed in CAD of the ions and reflects the dissociation from the excited species with a wide range of internal energy. The trapezoidal profile, on the other hand, is characteristic of the dissociation process from the state with a specific internal energy as is the case for the dissociation of the neutralized methanol, in which the excited methanol dissociates along a purely repulsive potential curve [39,49].

From the width at half maximum and the correction for the main beam width, we evaluated the kinetic energy release (KER) values for the ions $AgBr^-$ and Ag_2^- derived from Ag_2Br^+ as 0.12 and 0.73 eV, respectively. The KER value for Ag_2^- derived from Ag_3^+ is evaluated as 0.07 eV. These KER values correspond to the total kinetic energy released in the center of mass frame in the dissociation process of the excited cluster Ag_2Br^*. Using the thermochemical data shown in Figures 2 and 4, the energies available for the dissociation of Br or Ag from Ag_2Br^* are 1.4 and 2.49 eV, respectively and that of Ag from Ag_3^* is 0.41 eV. It is interesting to know that the KER value for the elimination of Br is much larger than that of Ag, though the corresponding available energy of Br loss is smaller than that of Ag loss.

The fraction of the KER values to the corresponding available energies for the elimination of Ag and Br from Ag_2Br^* are 5 and 52%, respectively. Efficiency for the internal to kinetic energy conversion is usually less than 15% for the elimination of atoms or small molecules [60]. While the fraction for Ag loss from Ag_2Br^* is in the right range of efficiency, that for Br loss is much larger than the efficiency expected. In the case of Ag loss from Ag_3^* a theoretical value for the fraction is 22% and experimental one is 5%. The fraction obtained using the theoretical value is larger than the fraction often found experimentally. The large available energy due to the low dissociation energy barrier presumed can explains this larger fraction for the dissociation of Ag_3^* into $Ag_2 + Ag$. Regarding the large fraction of 52% for the elimination of Br from Ag_2Br, the structure of Ag_2Br^+ is discussed below. The structures of Ag_2Br^* and Ag_3^* formed by the near resonant neutralization are considered to remain the same as those of the respective positive ions, since the neutralization is a Franck-Condon process. The structure of Ag_2Br^+ in the ground state is reported by Rabillioud to be an isosceles triangle ($AgBrAg^+$) whose apex angle is 111 degrees [36,37]. Since the loss of Ag from the isosceles triangular cluster $AgBrAg^*$ is expected to provide significant vibrational and rotational excitation in the Ag_2 fragment due to the large structural difference in the $AgBrAg^+$ ion and the ground state Ag_2. A value of 5% obtained for the KER fraction is reasonable. However, the large fraction of 52% in the elimination of Br cannot be explained from the isosceles triangular cluster $AgBrAg^*$ due to the larger structure difference than that of the Ag elimination. The available energies evaluated from the thermochemical data shown in Figure 2 are based on the formation of Ag_2 molecule and Br atom in their ground states. When the Ag_2 molecule is in an excited state, the available energy for the dissociation will decrease. The distance of Ag-Ag

in the triangular ion $AgBrAg^+$, reported by Rabilloud et al. [36,37] is evaluated to be 3.86×10^{-10} m from the Ag-Br bond length of 2.54×10^{-10} m and the apex angle of 111 degrees. When we employ a Morse potential with $D_e = 1.67$ eV and $r_e = 2.48 \times 10^{-10}$ m [61], the bond length of 3.86×10^{-10} m of the Ag_2 molecule corresponds to a potential energy higher than the vibrational ground state of Ag_2 by 1.28 eV. If this excitation energy of the fragment Ag_2 molecule is used to estimate the available energy, it becomes almost zero and, hence, the observed large KER value of 0.73 eV for the elimination of Br is too large to be explained by a reaction mechanism via precursor ion $AgBrAg^+$ in the lowest state. From the large KER value for the loss of Br, therefore, it is suggested that the precursor ion Ag_2Br^+ does not assume an isosceles triangular form but a scalene one of the type of $AgAgBr^+$, though the latter structure has not been confirmed by theoretical calculations. The excited neutral cluster $AgAgBr^*$ thus formed retains the same structure as that of $AgAgBr^+$ and is expected to provide a large KER value due to a single bond cleavage of AgAg-Br leading to the production of Ag_2 and Br.

4 Conclusion

In the high-energy CAD spectrum of Ag_2Br^+, the fragment peaks associated with the ions Ag^+, $AgBr^+$, and Ag_2^+ were dominantly observed, but the peak associated with Br^+ was scarcely observed. The dissociation channels of Ag_2Br in high-energy CAD were different from those found for the metastable dissociation. This difference was ascribed to the difference in the available amount of the internal energy of the produced excited precursor ion Ag_2Br^{+*}. It is suggested that the broad and higher internal energy of Ag_2Br^{+*} achieved in this work can provide many dissociation channels such as the elimination of Br, Ag, AgBr, and Ag_2.

In the charge inversion spectrum of Ag_2Br^+, the peaks associated with the ions $AgBr^-$ and Ag_2^- predominated, whereas the peak associated with the undissociated ion Ag_2Br^- was hardly observed. The peaks associated with Br^- and Ag^- were also observed, though the intensities of these ions were much weaker than those of Ag_2^- and $AgBr^-$. The dissociation behavior of the excited cluster Ag_2Br^* is in a good agreement with the calculated thermochemical data. The peak associated with Ag_2^- eliminated from Ag_2Br^+ is broad and the peak shape resembles a trapezoid. From the large KER value of 0.73 eV evaluated for Ag_2 in the charge inversion spectrum of Ag_2Br^+, the existence of a scalene triangular precursor ion $AgAgBr^+$ is suggested.

The fragment peaks associated with Ag^+ and Ag_2^+ were observed in the high-energy CAD spectrum of Ag_3^+, and the intensity of Ag^+ was much weaker than that of Ag_2^+. In contrast, in the low-energy CAD spectrum of Ag_3^+, Ag_2^+ was observed as a predominant fragment peak. The difference in the dissociation channel between the high-energy and low-energy CAD can be also understood by considering the internal energy distribution in Ag_3^{+*}.

In the charge inversion spectrum of Ag_3^+, the peaks associated with Ag^-, Ag_2^-, and Ag_3^- were observed, among which the undissociated Ag_3^- peak predominated. Whereas the internal energy of Ag_3^* calculated from the ionization potentials of Ag_3 and Cs was higher than the dissociation energy, the undissociated Ag_3^- peak was clearly observed. From the predominant existence of undissociated Ag_3^- in the charge inversion spectrum, it is suggested that the energy barrier for the dissociation into $Ag_2 + Ag$ is substantially higher than the energy level of Ag_3^* formed via near-resonant neutralization with the Cs target, though the energy barrier has not been calculated theoretically. From a comparison with the results reported by using the NeNePo measurement of Ag_3^-, we speculate that the Ag_3^* formed from the triangular ion Ag_3^+ by the near-resonant neutralization rearranges intramolecularly to the linear neutral cluster Ag_3 and is followed by negative ion formation on another collision with the Cs target without its appreciable dissociation.

This work was supported by Special Research Grant from Osaka Prefecture University, 2007.

References

1. J. Yoon, K.S. Kim, K.K. Baeck, J. Chem. Phys. **112**, 9335 (2000), and references therein
2. S.W. Buckner, J.R. Gord, B.S. Freiser, J. Chem. Phys. **88**, 3678 (1988)
3. J. Ho, K.M. Ervin, W.C. Lineberger, J. Chem. Phys. **93**, 6987 (1990)
4. C. Jackschath, I. Rabin, W. Schulze, Z. Phys. D **22**, 517 (1992)
5. H. Handschuh, C.-Y. Cha, P.S. Bechthold, G. Gantefor, W. Eberhardt, J. Chem. Phys. **102**, 6406 (1995)
6. V.A. Spasov, T.H. Lee, J.P. Maberry, K.M. Ervin, J. Chem. Phys. **110**, 5208 (1999)
7. S. Krückeberg, G. Dietrich, K. Lützenkirchen, L. Schweikhard, C. Walther, J. Ziegler, Int. J. Mass Spectom. Ion Process. **155**, 141 (1996)
8. A. Fielicke, I. Rabin, G. Meijer, J. Phys. Chem. A **110**, 8060 (2006)
9. S.P. Walch, C.W. Bauschlicher, S.R. Langhoff, J. Chem. Phys. **85**, 5900 (1986)
10. S.P. Walch, J. Chem. Phys. **87**, 6776 (1987)
11. C.W. Bauschlicher, S.R. Langhoff, H. Partridge, J. Chem. Phys. **91**, 2412 (1989)
12. K. Balasubramanian, P.Y. Feng, Chem. Phys. Lett. **159**, 452 (1989)
13. H. Partridge, C.W. Bauschlicher, S.R. Langhoff, Chem. Phys. Lett. **175**, 531 (1990)
14. V. Bonacic-Koutecky, L. Cespiva, P. Fantucci, J. Koutecky, J. Chem. Phys. **98**, 7981 (1993)
15. V. Bonacic-Koutecky, L. Cespiva, P. Fantucci, J. Pittner, J. Koutecky, J. Chem. Phys. **100**, 490 (1994)
16. R. Santamaria, I.G. Kaplan, O. Novaro, Chem. Phys. Lett. **218**, 395 (1994)
17. M.N. Huda, A.K. Ray, Eur. Phys. J. D **22**, 217 (2003)

18. Y. Wang, X.G. Gong, Eur. Phys. J. D **34**, 19 (2005)
19. D.P. de Bruijn, J. Neuteboom, V. Sidis, J. Los, Chem. Phys. **85**, 215 (1984); D.P. de Bruijn, J. Neuteboom, J. Los, Chem. Phys. **85**, 233 (1984)
20. J.C. Brenot, H. Dunet, J.A. Fayeton, M. Barat, M. Winter, Phys. Rev. Lett. **77**, 1246 (1996)
21. M. Barat, J.C. Brenot, H. Dunet, J.A. Fayeton, Y.J. Picard, Eur. Phys. J. D **1**, 271 (1998)
22. J.A. Fayeton, M. Barat, J.C. Brenot, H. Dunet, Y.J. Picard, U. Saalmann, R. Schmidt, Phys. Rev. A **57**, 1058 (1998)
23. M. Barat, J.C. Brenot, H. Dunet, J.A. Fayeton, Y.J. Picard, J. Chem. Phys. **110**, 10758 (1999)
24. M. Barat, J.C. Brenot, H. Dunet, J.A. Fayeton, Y.J. Picard, D. Babikov, M. Sizun, Chem. Phys. Lett. **306**, 233 (1999)
25. S. Hayakawa, Int. J. Mass Spectrom. Ion Process. **90**, 251 (1989)
26. S. Wolf, G. Sommerer, S. Rutz, E. Schreiber, T. Leisner, L. Woste, R.S. Berry, Phys. Rev. Lett. **74**, 4177 (1995)
27. D.W. Boo, Y. Ozaki, L.H. Andersen, W.C. Lineberger, J. Phys. Chem. A **101**, 6688 (1997)
28. T. Leisner, S. Vajda, S. Wolf, L. Woste, R.S. Berry, J. Chem. Phys. **111**, 1017 (1999)
29. H.O. Jeschke, M.E. Garcia, K.H. Bennemann, J. Phys. B: At. Mol. Opt. Phys. **29**, 545 (1996)
30. H.O. Jeschke, M.E. Garcia, K.H. Bennemann, Phys. Rev. A **54**, 4601 (1996)
31. M. Hartmann, J. Pittner, V. Bonacic-Koutecky, A. Heidenreich, J. Jortner, J. Chem. Phys. **108**, 3096 (1998)
32. M. Hartmann, A. Heidenreich, J. Pittner, V. Bonacic-Koutecky, J. Jortner, J. Phys. Chem. A **102**, 4069 (1998)
33. I. Andrianov, V. Bonacic-Koutecky, M. Hartmann, J. Manz, J. Pittner, K. Sundermann, Chem. Phys. Lett. **318**, 256 (2000)
34. J.M. L'Hermite, F. Rabilloud, L. Marcou, P. Labastie, Eur. Phys. J. D **14**, 323 (2001)
35. J.M. L'Hermite, F. Rabilloud, P. Labastie, F. Spiegelman, Eur. Phys. J. D **16**, 77 (2001)
36. F. Rabilloud, F. Spiegelmann, J.L. Heully, J. Chem. Phys. **111**, 8925 (1999)
37. F. Rabilloud, F. Spiegelman, J.M. L'Hermite, P. Labastie, J. Chem. Phys. **114**, 289 (2001)
38. S. Hayakawa, K. Harada, K. Arakawa, N. Morishita, J. Chem. Phys. **112**, 8432 (2000)
39. S. Hayakawa, Int. J. Mass Spectrom. **212**, 229 (2001)
40. R.G. Cooks, in *Collision Spectroscopy*, edited by R.G. Cooks (Prenum, New York, 1978), Chap. 7
41. S. Hayakawa, H. Endoh, K. Arakawa, N. Morishita, T. Sugiura, Int. J. Mass Spectom. Ion Process. **151**, 89 (1995)
42. S. Hayakawa, J. Mass Spectrom. **39**, 111 (2004)
43. S. Hayakawa, A. Kitaguchi, S. Kameoka, M. Toyoda, T. Ichihara, J. Chem. Phys. **124**, 224320 (2006)
44. P. Sharpe, C.J. Cassady, Chem. Phys. Lett. **191**, 111 (1992)
45. V.H. Wysocki, H.I. Kenttamaa, R.G. Cooks, Int. J. Mass Spectrom. Ion Process. **75**, 181 (1987)
46. K.L. Schey, H.I. Kenttämaa, V.H. Wysocki, R. Graham Cooks, Int. J. Mass Spectom. Ion Process. **90**, 71 (1989)
47. V.H. Wysocki, H.I. Kenttamaa, R.G. Cooks, J. Phys. Chem. **92**, 6465 (1988)
48. S.R. Horning, M. Vincenti, R.G. Cooks, J. Am. Chem. Soc. **112**, 119 (1990)
49. S. Hayakawa, K. Harada, N. Watanabe, K. Arakawa, N. Morishita, Int. J. Mass Spectrom. **202**, A1 (2000)
50. S. Hayakawa, K. Kadomura, M. Kimura, C.M. Dutta, Phys. Rev. A **70**, 022708 (2004)
51. S. Hayakawa, N. Terazawa, T. Sugiura, J. Phys. B **23**, 4539 (1990)
52. S. Hayakawa, N. Terazawa, T. Sugiura, J. Mass Spectrom. Soc. Jpn **41**, 225 (1993)
53. S. Hayakawa, M. Takahashi, K. Arakawa, N. Morishita, J. Chem. Phys. **110**, 2745 (1999)
54. S. Hayakawa, K. Tomozawa, T. Takeuchi, K. Arakawa, N. Morishita, Phys. Chem. Chem. Phys. **5**, 2386 (2003)
55. S. Hayakawa, N. Kabuki, Eur. Phys. J. D **38**, 163 (2006)
56. S. Hayakawa, M. Hashimoto, H. Matsubara, F. Turecek, J. Am. Chem. Soc. **129**, 7936 (2007)
57. S. Hayakawa, K. Taguchi, R. Kotani, K. Arakawa, N. Morishita, J. Mass Spectrom. Soc. Jpn **49**, 219 (2001)
58. S. Hayakawa, H. Matsubara, Y. Kawamura, K. Iwamoto, Int. J. Mass Spectrom. **262**, 220 (2007)
59. S. Hayakawa, Y. Kawamura, Y. Takahashi, Int. J. Mass Spectrom. **246**, 56 (2005)
60. R.G. Cooks, J.H. Beynon, R.M. Caprioli, G.R. Lester, *Metastable Ions* (Elsevier, Amsterdam, 1973)
61. K.P. Huber, G. Herzberg, *Molecular Spectra and Molecular Structure IV. Constants of Diatomic Molecules* (Van Nostrand Reinhold, New York, 1979)